

TMD parton showers for associated $\gamma + \text{jet}$ production in electron-proton collisions at high energies

A.V. Lipatov^{1,2}, M.A. Malyshev¹

May 10, 2023

¹*Skobeltsyn Institute of Nuclear Physics, Lomonosov Moscow State University, 119991, Moscow, Russia*

²*Joint Institute for Nuclear Research, 141980, Dubna, Moscow region, Russia*

Abstract

An earlier developed k_T -factorization framework to calculate the associated prompt photon and hadronic jets production cross sections at high energies is extended now to the electron-proton deep inelastic scattering. The proposed method is based on joint usage of the PEGASUS and CASCADE Monte-Carlo event generators, which deal with the transverse momentum dependent (TMD) gluon and quark densities in a proton. First of them, PEGASUS, is applied to produce off-shell photon-gluon fusion events. Then, to properly simulate the kinematics of the produced jets, the TMD parton shower algorithm implemented into the CASCADE is used. We demonstrate basic features of the approach considering latest H1 and ZEUS data on prompt photon plus jet production at low Q^2 collected at HERA. We achieve a good description of the measurements and point out that a correct simulation of parton showers is essential for studying non-inclusive processes at high energies within the TMD-based approaches.

Keywords: deep inelastic scattering, high energy factorization, CCFM evolution, TMD gluon density, prompt photon production

1 Introduction

Inclusive prompt photon¹ production at high energies is an important subject of investigation at modern colliders, such as LHC. Being quite clean in sense of final state effects, these processes can serve as an important source of information about the proton structure (expressed in terms of parton density functions) and represent an important background to many processes involving photons in the final state, including Higgs boson production. Also, a rather clear and robust way to study parton content of a proton can be provided by the prompt photon photoproduction in deep inelastic ep scattering (DIS), where the exchanged photon is of small virtuality $Q^2 \lesssim 1 \text{ GeV}^2$ [1–3]. In fact, the corresponding cross section at leading order (LO) of perturbative QCD is mainly governed by the direct $\gamma + q \rightarrow \gamma + q$ and several resolved photon subprocesses, where the photon emitted by the electron fluctuates into a hadronic state. A gluon and/or a quark of this hadronic fluctuation takes part then in hard interactions². Including into the consideration accompanying final state jet(s) gives an opportunity to study jet observables, different photon-jet correlations, thus allowing to test the production dynamics in many additional aspects. Investigation of prompt photon production will be an important part of the physical program at future electron-proton or electron-ion colliders, such as LHeC [4], FCC-eh [5], Eic [6] and EIC [7]. Thus, relevant theoretical studies and developing corresponding Monte-Carlo event generators are rather important tasks at present.

Usually, a theoretical description of prompt photon photoproduction relies on conventional (collinear) QCD factorization, which is based on well-known Dokshitzer-Gribov-Lipatov-Altarelli-Parisi (DGLAP) quark and gluon evolution equations [8]. Within this formalism, next-to-leading order (NLO) calculations are available [9–11]. The prompt photon production events can be produced also with some Monte-Carlo generators, such as PYTHIA [12] or HERWIG [13]. Alternative calculations can be done in the framework of high-energy factorization [14] or k_T -factorization approach [15] based on Balitsky-Fadin-Kuraev-Lipatov (BFKL) [16] or Catani-Ciafaloni-Fiorani-Marchesini (CCFM) [17] gluon evolution equations. The k_T -factorization QCD approach has certain technical advantages in the ease of including higher-order pQCD radiative corrections corresponding to real initial-state gluon emissions (namely, terms, proportional to $\alpha_s^n \ln^n s / \Lambda_{\text{QCD}}^2 \sim \alpha_s^n \ln^n 1/x$, important at high energies s , or small x) in the form of transverse momentum dependent (TMD, or unintegrated) gluon density (see review [18] for more information).

Studies of prompt photon production within the k_T -factorization approach have their own long history (see, for example, [19–28] and references therein). Moreover, such processes have been also investigated [29–37] in the framework of Color Glass Condensate (CGC) formalism [38–40]. In particular, a good description of experimental data for inclusive production events was obtained for both electron-proton [19–21] and proton-proton collisions [26–28]. A simple model [41] to reconstruct the jet kinematics in associated $\gamma + \text{jet}$ production was applied [25] and necessity for correct reconstruction of this kinematics was pointed out. The latter is a special task for any calculations where the non-collinear QCD evolution of the initial parton (gluon) cascade is used. In the case of CCFM evolution, a method based on numerical simulation of TMD parton showers was proposed [42] and successfully applied to associated $\gamma + \text{jet}$ production at LHC [27]. In fact, earlier description of the experimental data was significantly improved. Here we extend the consideration to electron-proton collisions and analyse latest HERA data [1–3]

¹Photons are considered as prompt if they are produced in the hard interaction subprocess rather than in hadron decays or via fragmentation.

²Beyond the LO, the difference between these two mechanisms disappears.

on prompt photon and associated jet photoproduction taken by the H1 and ZEUS Collaborations at $\sqrt{s} = 319$ GeV.

The paper is organized as follows. In Section 2 we briefly describe our approach. In Section 3 we present our numerical results and compare them with available HERA data. Section 4 contains our conclusions.

2 Theoretical framework

Let us shortly describe the main calculation steps. In the photoproduction regime the colliding electron emits a quasi-real ($Q^2 \sim 0$) photon, so one deals then with photon-proton interaction:

$$d\sigma(ep \rightarrow e'\gamma X) = \int f_{\gamma/e}(y) d\sigma(\gamma p \rightarrow \gamma X) dy, \quad (1)$$

where y is the fraction of initial electron energy carried by the photon in the laboratory frame. We use the well-known Weizacker-Williams approximation for bremsstrahlung photon distribution from the electron:

$$f_{\gamma/e}(y) = \frac{\alpha}{2\pi} \left(\frac{1 + (1-y)^2}{y} \ln \frac{Q_{\max}^2}{Q_{\min}^2} + 2m_e^2 y \left(\frac{1}{Q_{\max}^2} - \frac{1}{Q_{\min}^2} \right) \right), \quad (2)$$

where m_e is the electron mass, $Q_{\min}^2 = m_e^2 y^2 / (1-y)^2$ and $Q_{\max}^2 = 1$ GeV², which is a typical value for photoproduction measurements at the HERA.

As it was already mentioned above, direct contribution to the prompt photon photoproduction comes from the $\mathcal{O}(\alpha^2)$ deep inelastic Compton scattering subprocess, $\gamma + q \rightarrow \gamma + q$. In the consideration below we decompose the quark content of a proton into the sea and valence parts and exploit the idea that the sea quarks all appear from a perturbative chain as a result of the QCD evolution of gluon density³. Then, appending an explicit gluon splitting vertex, we come to the $\mathcal{O}(\alpha^2 \alpha_s)$ photon-gluon fusion subprocess

$$\gamma(k_1) + g^*(k_2) \rightarrow \gamma(p) + q(p_1) + \bar{q}(p_2). \quad (3)$$

Here q denotes any quark flavor and the particles four-momenta are given in parentheses. The subprocess (3) covers also the main part of LO resolved photon contributions. We employ the k_T -factorization approach, thus effectively taking into account a large piece of higher-order pQCD corrections via CCFM-evolved TMD gluon density in a proton. In this way, we keep the non-zero virtuality of the incoming gluon, $k_2^2 \simeq k_{2T}^2 = -\mathbf{k}_{2T}^2 \neq 0$. The corresponding off-shell production amplitude was calculated in [21] and is implemented now in the Monte-Carlo generator PEGASUS [43]. We note that the subprocess (3), being supplemented with the final state parton radiation, covers (at least partly) many other off-shell subprocesses — for example, $\gamma + q^* \rightarrow \gamma + q + g$, which has been taken into account in our previous calculations [21] separately. The effects of initial and final state parton emissions (ISR and FSR) can be simulated using the standard parton showering algorithms, such as implemented into CASCADE or PYTHIA. The remaining contributions from valence quarks, important at large x , are taken into account via simple $\mathcal{O}(\alpha^2)$ deep inelastic Compton scattering subprocess. Of course, here one can safely neglect the off-shellness of valence quarks and employ the conventional (collinear) QCD factorization. Additionally we will take into account $\mathcal{O}(\alpha^2 \alpha_s^2)$ box contribution:

$$\gamma(k_1) + g^*(k_2) \rightarrow \gamma(p_1) + g(p_2), \quad (4)$$

³A similar treatment has been used recently in the prompt photon hadroproduction case [28].

since it is known to be sizeable due to high gluon luminosity at small x . Here we improve the previous consideration [21] by taking into account non-zero transverse momentum of initial gluon and use analytical expressions [24] for off-shell production amplitude⁴, where the one-loop integrals were evaluated with QCDLOOP [44].

To calculate the photon-proton interaction cross section in the k_T -factorization QCD approach one has to convolute the corresponding partonic cross section with the TMD gluon density in a proton $f_g(x, \mathbf{k}_T^2, \mu^2)$:

$$d\sigma(\gamma p \rightarrow \gamma X) = \int \frac{dx_2}{x_2} \frac{d\phi_2}{2\pi} d\mathbf{k}_{2T}^2 f_a(x_2, \mathbf{k}_{2T}^2, \mu^2) d\hat{\sigma}(\gamma g^* \rightarrow \gamma X), \quad (5)$$

where x_2 and ϕ_2 are the longitudinal momentum fraction of the colliding proton carried by incoming off-shell gluon and its azimuthal angle, respectively. To avoid the collinear divergencies appearing in (3) when the final photon becomes collinear to the outgoing quark, we follow an approach [23] and split the cross section into two pieces:

$$\sigma = \sigma_{\text{pert}}(\mu_{\text{reg}}^2) + \sigma_{\text{non-pert}}(\mu_{\text{reg}}^2), \quad (6)$$

where $\sigma_{\text{pert}}(\mu_{\text{reg}}^2)$ is the perturbative contribution calculated under usual condition when the wavelength of produced photon (in the emitting quark rest frame) becomes larger than the typical hadronic scale, $\mathcal{O}(1 \text{ GeV}^{-1})$. Below this scale, different non-perturbative effects, including photon fragmentation, have to be taken into account. To separate these two pieces the regularization scale μ_{reg} is used. Following [23], we restrict $\sigma_{\text{pert}}(\mu_{\text{reg}}^2)$ to the region $M \geq \mu_{\text{reg}}$, where M is the invariant mass of the photon + quark subsystem and $\mu_{\text{reg}} \sim 1 \text{ GeV}$ is the hadronic scale. Under this condition, the contribution $\sigma_{\text{pert}}(\mu_{\text{reg}}^2)$ is free from collinear divergences. Moreover, a special photon isolation criterion (so-called cone isolation), introduced in experimental analyses [1–3], in our calculations is used as a tool⁵ to remove the non-perturbative part $\sigma_{\text{non-pert}}(\mu_{\text{reg}}^2)$, where the final photon is radiated close to the quark (inside the isolation cone). The sensitivity of the numerical results to μ_{reg} is reasonably soft if the photon isolation condition is applied (see [23] for more information). We note also that under this condition the fragmentation contributions become negligible [1–3], so we can safely omit it in the consideration below.

Concerning the TMD gluon density, in the present paper we have tested two latest sets obtained from the numerical solution of CCFM evolution equation. First of them is the JH'2013 set 2 [46], which is widely used in phenomenological applications (see, for example, [27, 28, 47] and references therein). The parameters of the corresponding (rather empirical) initial gluon density were derived from a fit to precision HERA data on the proton structure functions $F_2(x, Q^2)$ and $F_2^c(x, Q^2)$ at $x < 5 \cdot 10^{-3}$ and $Q^2 > 3.5 \text{ GeV}^2$. Also we have tried a very recent TMD gluon distribution in a proton, namely, LLM'2022 [48]. In contrast with JH'2013 set 2, the analytical expression for the starting distribution was chosen in a more physically motivated way — namely, from the best description of the LHC data on charged hadron production at low transverse momenta $p_T \sim 1 \text{ GeV}$ in the framework of modified soft quark-gluon string model (QGSM) [49, 50]. Moreover, the gluon saturation effects, which are important at low scales, were taken into account. Some phenomenological parameters were determined from the LHC and HERA data on several hard QCD processes (see [48, 51] for more information). Both these TMD gluon densities are available in the Monte-Carlo event generator PEGASUS and popular TMDLIB

⁴We would like to note that the expression given in the Appendix of [24] is a bit misleading. Namely, the denominator of (A5) from [24] must be taken universal for the helicity amplitudes (A1) — (A3); alternatively, one can multiply (A9) by $(u + t_1)/(s + t_1)$.

⁵Another photon isolation criterion was also proposed [45].

package [52], which is a C++ library providing a framework and an interface to the different parametrizations.

A last important point of our calculations is connected with the proper determination of the associated jet momentum. In fact, the quarks and/or gluons produced in the hard subprocesses described above can form final state hadronic jets. However, in addition to that, the produced photon is accompanied by a number of gluons radiated in the course of the non-collinear evolution, which also give rise to final jets. This is a distinct and remarkable feature of the CCFM-based approach used. From all of the hadronic jets we choose the one, carrying the largest transverse momentum and satisfying the experimental cuts (leading jet) and then compute the cross section of $\gamma + \text{jet}$ production. Technically, we produce a Les Houches Event file [53] in the parton level calculations performed using the PEGASUS and then process the file with the TMD shower routine implemented into the Monte-Carlo event generator CASCADE [54]. This routine only recently became available for DIS processes, so our work presents the first application of this procedure to photoproduction processes at HERA, to the best of our knowledge. Thus, we fully reconstruct the CCFM evolution ladder. The hadronic jets are reconstructed with the k_T -algorithm, implemented in the FASTJET tool [55]. This method gives us the possibility to take into account the contributions from initial state parton showers in a consistent way. Moreover, it was successfully applied already to investigate prompt photon (or Higgs boson) and associated jet production at the LHC (see [27, 47]). Note that additionally we performed final state hadronization procedure, which is necessary to fully reproduce the experimental setup [1–3].

3 Numerical results

Now we are in a position to present the numerical results. First we describe our input and kinematical conditions. So, as it is often done, we set the renormalization scale μ_R equal to the produced photon transverse energy E_T^γ . The factorization scale is defined as $\mu_F^2 = \hat{s} + \mathbf{Q}^2$ with \hat{s} and \mathbf{Q}_T being the subprocess invariant energy and net transverse momentum of the initial state, respectively. Note that the definition of μ_F is dictated mainly by the CCFM evolution algorithm (see [17]). Then, we use the massless limit for light (u , d and s) quarks and set the charm and beauty masses to $m_c = 1.28$ GeV and $m_b = 4.75$ GeV. Also, we apply the two-loop formula for the strong coupling constant α_s with $N_f = 4$ quark flavours at $\Lambda_{\text{QCD}} = 200$ MeV, as it was originally done in the fits [46, 48].

The experimental data for associated prompt photon and jet photoproduction at HERA were taken by both the H1 and ZEUS collaborations. The H1 data [1] were obtained in the following kinematical region⁶: $6 < E_T^\gamma < 15$ GeV, $E_T^{\text{jet}} > 4.5$ GeV, $-1.0 < \eta^\gamma < 2.4$, $-1.3 < \eta^{\text{jet}} < 2.3$. The fraction y of the electron energy transferred to the photon is restricted to the range $0.1 < y < 0.7$. More recent ZEUS measurements [2, 3] refer to the region defined by $6 < E_T^\gamma < 15$ GeV, $4 < E_T^{\text{jet}} < 35$ GeV, $-0.7 < \eta^\gamma < 0.9$, $-1.5 < \eta^{\text{jet}} < 1.8$ and $0.2 < y < 0.7$. The data [1–3] were obtained with the electron energy $E_e = 27.6$ GeV and proton energy $E_p = 920$ GeV.

Our results are compared with experimental data in Figs. 1 — 8. So, the transverse energy E_T^γ , E_T^{jet} and pseudorapidity η^γ , η^{jet} distributions of the produced photon and jet are shown in Figs. 1 and 2. We find that the calculations based on recently proposed LLM’2022 gluon density (represented by the green histograms) are consistent with

⁶Here and in the following all kinematic quantities are given in the laboratory frame with positive OZ axis direction given by the proton beam.

the H1 data in most bins, although some discrepancies are present. In particular, these predictions tend to underestimate the H1 measurements at low E_T^{jet} and rear photon pseudorapidity η^γ , although coincide with the data within the theoretical and experimental uncertainties. Note that theoretical uncertainties of our calculations are estimated in a traditional way, varying the renormalization scale⁷ around its default value as $\mu_R \rightarrow \xi\mu_R$ with $\xi = 1/2$ or 2. One can see that the obtained results reproduce behavior of the measured η^{jet} spectrum (shifted towards positive pseudorapidities), which could not be achieved in earlier calculations [21, 24]. This is a direct consequence of the applied method of proper determination of jet kinematics based on the TMD shower algorithm. Similar conclusions were already done in [27, 47] where production of prompt photons or Higgs bosons associated with hadronic jet(s) in pp collisions at the LHC was studied. Overall agreement of our predictions with more recent ZEUS data is a bit worse, but still rather reasonable (see Fig. 2). Although there is some overestimation of the data at low E_T^γ , large E_T^{jet} and low separation in azimuthal angle between the produced photon and jet, $\Delta\phi$, the shapes of η^{jet} and $\Delta\eta = \eta^\gamma - \eta^{\text{jet}}$ spectra are reproduced well. These observables are sensitive to the proper determination of jet kinematics.

As it has been mentioned above, to investigate the dependence of our results on the TMD gluon density in a proton, we have repeated the calculations using another set, JH'2013 set 2. In contrast with LLM'2022, it leads to systematic overestimation of the HERA data, that coincides with the observation of [51]. It was argued [48, 51] that better agreement achieved with the LLM'2022 is an immediate consequence of using a physically motivated expression for the corresponding starting distribution. Thus, our calculations demonstrate that the HERA data on associated $\gamma + \text{jet}$ production in DIS are sensitive to the TMD gluon densities and could help to clearly distinguish the latter. It could be important for experiments at future electron-proton or electron-ion colliders, such as LHeC, FCC-eh, EIC and EIC. Additionally, we find that contribution from the valence quarks is negligible in the considered kinematical region.

For comparison we also show results of conventional NLO pQCD calculations taken from [1–3]. These predictions are slightly below the LLM'2022 ones but rather close to them for most of observables within the uncertainties. The NLO pQCD calculations also tend to underestimate the H1 data. However, they agree well with both the H1 and ZEUS measurements at large E_T^{jet} and small $\Delta\phi < 90^\circ$. The JH'2013 set 2 gluon density significantly overshoots the NLO pQCD results.

Other important variables are the longitudinal momenta fractions carried by the colliding partons. The momentum fractions of the initial photon and proton are introduced in the ZEUS analyses [2, 3] as the following:

$$x_\gamma^{\text{obs}} = \frac{E_T^\gamma e^{-\eta^\gamma} + E_T^{\text{jet}} e^{-\eta^{\text{jet}}}}{2yE_e}, \quad x_p^{\text{obs}} = \frac{E_T^\gamma e^{\eta^\gamma} + E_T^{\text{jet}} e^{\eta^{\text{jet}}}}{2E_p}. \quad (7)$$

At $x_\gamma^{\text{obs}} > 0.8$ the cross section is believed to be dominated by the "direct photon" contributions, whereas at lower x_γ^{obs} the "resolved photon" contributions play the main role. The H1 Collaboration refers to x_γ^{LO} and x_p^{LO} estimators given by [1]:

$$x_\gamma^{\text{LO}} = \frac{E_T^\gamma (e^{-\eta^\gamma} + e^{-\eta^{\text{jet}}})}{2yE_e}, \quad x_p^{\text{LO}} = \frac{E_T^\gamma (e^{-\eta^\gamma} + e^{\eta^{\text{jet}}})}{2E_p}. \quad (8)$$

The x_γ^{LO} and x_p^{LO} variables explicitly use only of the photon energy, which is better measured than the jet energy. Our predictions for these observables are shown in Fig. 3.

⁷In the CCFM-based approach, the factorization scale μ_F is related with the evolution variable and therefore should not be varied. See [17] for more details.

We find that results obtained with LLM'2022 gluon density agree well with the H1 data. In contrast with earlier calculations [21], they show more smeared cross sections for the x_γ^{obs} and x_γ^{LO} spectra, which is in a better agreement with the data. Again, this is due to more accurate determination of the jet kinematics compared to the previous considerations. However, there is still some overestimation of the ZEUS data at small x_γ^{obs} and large x_p^{obs} .

Although we cannot distinguish between the "resolved photon" and "direct photon" contributions, the dedicated study of cross sections measured at low and high x_γ^{obs} can provide an additional test of theoretical calculations. In fact, in our simulations different interplay between the subprocesses (3) and (4) can result then in different cross sections in these two regions and thus there might be a deviation from the data. To investigate it in more details, we have performed the calculations at low $x_\gamma^{\text{obs}}(x_\gamma^{\text{LO}}) < 0.8$ and high $x_\gamma^{\text{obs}}(x_\gamma^{\text{LO}}) > 0.8$ values and compared our results with the H1 [1] and ZEUS [3] measurements, see Figs. 4 — 8. One can see that transverse energy E_T^γ , E_T^{jet} and pseudorapidity η^γ , η^{jet} spectra predicted by the LLM'2022 gluon density are in a reasonable agreement with the ZEUS data [3] in the both these kinematical regions within the uncertainties, except only last E_T^{jet} and forward η^{jet} bins at $x_\gamma^{\text{obs}} < 0.8$. However, there is some overestimation of the ZEUS data at large $x_p^{\text{obs}} \geq 0.015$, that is clearly visible at $x_\gamma^{\text{obs}} < 0.8$. It comes from the events where the produced photon and jet are close to each other, as one can see from $\Delta\phi$ distributions shown in Fig. 7. Note that our predictions overshoot the ZEUS data on $\Delta\phi$ spectra at $\Delta\phi < 150^\circ$ and $x_\gamma^{\text{obs}} > 0.8$, but agree well with the H1 measurements which were performed in the similar kinematical region. In contrast, at low $x_\gamma^{\text{obs}} < 0.8$ the H1 data for $\Delta\phi$ distributions are clearly underestimated everywhere while corresponding ZEUS data are reasonably well described. Therefore, at this point it could be some contradiction between the H1 and ZEUS measurements. In any case, special studies of transverse correlations between the final state particles are known to be useful to investigate the production dynamics (see, for example, [19–21, 25] and references therein). So, the H1 Collaboration has investigated the distribution on the component of the photon's momentum perpendicular to the jet direction in the transverse plane, $p_\perp = |\mathbf{p}_T^\gamma \times \mathbf{p}_T^{\text{jet}}|/|\mathbf{p}_T^{\text{jet}}| = E_T^\gamma \sin \Delta\phi$. Similar to $\Delta\phi$ spectra, the distribution over p_\perp is particularly sensitive to the higher-order pQCD corrections⁸, which are taken into account in the form of CCFM-evolved TMD gluon densities in our calculations. The predictions for p_\perp spectra are confronted with the H1 data in Fig. 8. We find that k_T -factorization results agree well with the H1 data in the "direct photon" region, although LLM'2022 gluon slightly underestimates the data at low p_\perp and JH'2013 set 2 tends to overshoots the latter. The conventional NLO pQCD calculations do not reproduce the H1 data both in the normalization and shape. At the same time we find that none of the calculations is able to describe the overall normalization of the data at $x_\gamma^{\text{LO}} < 0.8$, although the shape of measured distribution is reproduced well by all of them. Thus, further investigation of such an observable could be important to discriminate between the different approaches.

Finally, we can conclude that the LLM'2022 predictions reproduce well the latest HERA data for most of the observables within the theoretical and experimental uncertainties. It is due to more accurate determination of jet kinematics in our consideration compared to earlier analyses performed within the TMD-based approaches. These calculations are rather close to the NLO pQCD ones at $x_\gamma^{\text{obs}} > 0.8$ and tend to lie above the latter at $x_\gamma^{\text{obs}} < 0.8$. The NLO pQCD provides a better description of the jet transverse energy spectra, but unable to reproduce well the data on most of correlation variables (such as p_\perp ones). The JH'2013 set 2 gluon density overshoots the HERA data, although at $x_\gamma^{\text{obs}} < 0.8$ the difference between these predictions and LLM'2022 ones become smaller.

⁸In the conventional (collinear) LO approximation, it must be simply a delta function since the produced photon and the jet are back-to-back in the transverse plane.

So, the cross sections of associated $\gamma + \text{jet}$ production in DIS events are sensitive to the TMD gluon density in a proton and can be used to constrain it.

4 Conclusion

We have considered associated production of prompt photon and hadronic jets in photoproduction regime of deep inelastic electron-proton scattering at high energies. The calculations were performed in the framework of k_T -factorization QCD approach and mainly based on two off-shell photon-gluon fusion subprocesses, $\gamma + g^* \rightarrow \gamma + q + \bar{q}$ and $\gamma + g^* \rightarrow \gamma + g$, implemented now into the Monte-Carlo generator PEGASUS. First of them, being supplemented with effects of the final-state parton radiation, covers many other subprocesses, including resolved photon contributions. An additional valence quark-induced subprocess $\gamma + q_{\text{val}} \rightarrow \gamma + q$, which can be important at large x region, has been taken into account in the conventional (collinear) QCD factorization. In the numerical calculations we have tested two CCFM-evolved gluon distributions in a proton, namely, JH'2013 set 2 and very recent LLM'2022 gluon, both available in PEGASUS and TMDLIB packages. The LLM'2022 gluon density is based on simultaneous fit to the number of HERA and LHC processes sensitive to the gluon content of the proton. To reconstruct correctly the kinematics of the hadronic jets the TMD parton shower implemented into the Monte-Carlo generator CASCADE has been applied for the first time for the DIS process.

We have achieved reasonably good agreement between our predictions obtained with the recent LLM'2022 gluon density in a proton and latest H1 and ZEUS experimental data, thus demonstrating again the importance of initial state TMD parton showers for jet determination in the TMD-based approaches. The previously developed framework to calculate the jet associated processes is extended now to the electron-proton deep inelastic scattering. It is important for forthcoming studies at future electron-proton and electron-ion colliders, such as LHeC, FCC-he, EIC and EIC.

The next version of Monte-Carlo event generator PEGASUS (1.08), which is extended now to the considered DIS process, will be released shortly.

Acknowledgements

We thank S.P. Baranov and G.I. Lykasov for their important comments and remarks. We are also grateful to H. Jung for help with implementation of CASCADE in DIS. Framework setting, matrix elements adaptation and the analysis of the results were supported by the grant of the Foundation for the Advancement of Theoretical Physics and Mathematics “BASIS” 20-1-3-11-1. Work on implementation of parton showers and hadronization for photoproduction processes were supported by the Russian Science Foundation under grant 22-22-00119.

References

- [1] H1 Collaboration, Eur. Phys. J. C **66**, 17 (2010).
- [2] ZEUS Collaboration, Phys. Lett. B **730**, 293 (2014).
- [3] ZEUS Collaboration, JHEP **1408**, 023 (2014).
- [4] LHeC Collaboration and FCC-he Study Group, J. Phys. G: Nucl. Part. Phys. **48**, 110501 (2021).

- [5] FCC Collaboration, Eur. Phys. J. C **79**, 474 (2019).
- [6] R. Abdul Khalek et al., Nucl. Phys. A **1026**, 122447 (2022).
- [7] D.P. Anderle et al., Front. Phys. **16**, 64701 (2021).
- [8] V.N. Gribov, L.N. Lipatov, Sov. J. Nucl. Phys. **15**, 438 (1972);
L.N. Lipatov, Sov. J. Nucl. Phys. **20**, 94 (1975);
G. Altarelli, G. Parisi, Nucl. Phys. B **126**, 298 (1977);
Yu.L. Dokshitzer, Sov. Phys. JETP **46**, 641 (1977).
- [9] M. Fontannaz, J.Ph. Guillet, G. Heinrich, Eur. Phys. J. C **21**, 303 (2001).
- [10] M. Fontannaz, G. Heinrich, Eur. Phys. J. C **34**, 191 (2004).
- [11] A. Zembrzuski, M. Krawczyk, arXiv:hep-ph/0309308.
- [12] T. Sjöstrand, S. Ask, J.R. Christiansen, R. Corke, N. Desai, P. Ilten, S. Mrenna, S. Prestel, C.O. Rasmussen, P.Z. Skands, Comput. Phys. Commun. **191**, 159 (2015).
- [13] J. Bellm, S. Gieseke, D. Grellscheid, S. Plätzer, M. Rauch, C. Reuschle, P. Richardson, P. Schichtel, M.H. Seymour, A. Siodmok, A. Wilcock, N. Fischer, M.A. Harrendorf, G. Nail, A. Papaefstathiou, D. Rauch, Eur. Phys. J. C **76**, 196 (2016).
- [14] S. Catani, M. Ciafaloni, F. Hautmann, Nucl. Phys. B **366**, 135 (1991);
J.C. Collins, R.K. Ellis, Nucl. Phys. B **360**, 3 (1991).
- [15] L.V. Gribov, E.M. Levin, M.G. Ryskin, Phys. Rep. **100**, 1 (1983);
E.M. Levin, M.G. Ryskin, Yu.M. Shabelsky, A.G. Shuvaev, Sov. J. Nucl. Phys. **53**, 657 (1991).
- [16] E.A. Kuraev, L.N. Lipatov, V.S. Fadin, Sov. Phys. JETP **44**, 443 (1976);
E.A. Kuraev, L.N. Lipatov, V.S. Fadin, Sov. Phys. JETP **45**, 199 (1977);
I.I. Balitsky, L.N. Lipatov, Sov. J. Nucl. Phys. **28**, 822 (1978).
- [17] M. Ciafaloni, Nucl. Phys. B **296**, 49 (1988);
S. Catani, F. Fiorani, G. Marchesini, Phys. Lett. B **234**, 339 (1990);
S. Catani, F. Fiorani, G. Marchesini, Nucl. Phys. B **336**, 18 (1990);
G. Marchesini, Nucl. Phys. B **445**, 49 (1995).
- [18] R. Angeles-Martinez, A. Bacchetta, I.I. Balitsky, D. Boer, M. Boggione, R. Boussarie, F.A. Ceccopieri, I.O. Cherednikov, P. Connor, M.G. Echevarria, G. Ferrera, J. Grados Luyando, F. Hautmann, H. Jung, T. Kasemets, K. Kutak, J.P. Lansberg, A. Lelek, G.I. Lykasov, J.D. Madrigal Martinez, P.J. Mulders, E.R. Nocera, E. Petreska, C. Pisano, R. Placakyte, V. Radescu, M. Radici, G. Schnell, I. Scimemi, A. Signori, L. Szymanowski, S. Taheri Monfared, F.F. Van der Veken, H.J. van Haevermaet, P. Van Mechelen, A.A. Vladimirov, S. Wallon, Acta Phys. Polon. B **46**, 2501 (2015).
- [19] A.V. Lipatov, N.P. Zotov, Phys. Rev. D **72**, 054002 (2005).
- [20] A.V. Lipatov, N.P. Zotov, Phys. Rev. D **81**, 094027 (2010).
- [21] A.V. Lipatov, M.A. Malyshev, N.P. Zotov, Phys. Rev. D **88**, 074001 (2013).
- [22] T. Pietrycki, A. Szczurek, Phys. Rev. D **76**, 034003 (2007).

- [23] S.P. Baranov, A.V. Lipatov, N.P. Zotov, Phys. Rev. D **78**, 014025 (2008).
- [24] B.A. Kniehl, M.A. Nefedov, V.A. Saleev, Phys. Rev. D **89**, 114016 (2014).
- [25] A.V. Lipatov, N.P. Zotov, Phys. Rev. D **90**, 094005 (2014).
- [26] A.V. Lipatov, M.A. Malyshev, Phys. Rev. D **94**, 034020 (2016).
- [27] A.V. Lipatov, M.A. Malyshev, H. Jung, Phys. Rev. D **100**, 034028 (2019).
- [28] K. Golec-Biernat, L. Motyka, T. Stebel, Phys. Rev. D **103**, 034013 (2021).
- [29] J. Jalilian-Marian, A.H. Rezaeian, Phys. Rev. D **86**, 034016 (2012).
- [30] S. Benic, K. Fukushima, Nucl. Phys. A **958**, 1 (2017).
- [31] S. Benic, K. Fukushima, O. Garcia-Montero, R. Venugopalan, JHEP **1701**, 115 (2017).
- [32] S. Benic, K. Fukushima, O. Garcia-Montero, R. Venugopalan, Phys. Lett. B **791**, 11 (2019).
- [33] B. Ducloue, T. Lappi, H. Mäntysaari, Phys. Rev. D **97**, 054023 (2018).
- [34] G. Sampaio dos Santos, G. Gil da Silveira, M. Machado, Eur. Phys. J. C **80**, 812 (2020).
- [35] V.P. Goncalves, Y. Lima, R. Pasechnik, M. Sumnera, Phys. Rev. D **101**, 094019 (2020).
- [36] I. Kolbe, K. Roy, F. Salazar, B. Schenke, R. Venugopalan, JHEP **2021**, 52 (2021).
- [37] P. Caucal, F. Salazar, B. Schenke, T. Stebel, R. Venugopalan, arXiv:2304.03304.
- [38] L.D. McLerran, R. Venugopalan, Phys. Rev. D **49**, 2233 (1994).
- [39] L.D. McLerran, R. Venugopalan, Phys. Rev. D **49**, 3352 (1994).
- [40] L.D. McLerran, R. Venugopalan, Phys. Rev. D **50**, 2225 (1994).
- [41] S.P. Baranov, N.P. Zotov, Phys. Lett. B **491**, 111 (2000).
- [42] S. Dooling, F. Hautmann, H. Jung, Phys. Lett. B **736**, 293 (2014).
- [43] A.V. Lipatov, M.A. Malyshev, S.P. Baranov, Eur. Phys. J. C **80**, 330 (2020).
- [44] R.K. Ellis, G. Zanderighi, JHEP **0802**, 002 (2008).
- [45] S. Frixione, Phys. Lett. B **429**, 369 (1998).
- [46] F. Hautmann, H. Jung, Nucl. Phys. B **883**, 1 (2014).
- [47] A.V. Lipatov, M.A. Malyshev, Phys. Rev. D **103**, 094021 (2020).
- [48] A.V. Lipatov, G.I. Lykasov, M.A. Malyshev, Phys. Rev. D **107**, 014022 (2023).
- [49] V.A. Bednyakov, G.I. Lykasov, V.V. Lyubushkin, Europhys. Lett. **92**, 31001 (2010).

- [50] V.A. Bednyakov, A.A. Grinyuk, G.I. Lykasov, M. Poghosyan, *Int. J. Mod. Phys. A* **27**, 1250042 (2012).
- [51] A.V. Lipatov, G.I. Lykasov, M.A. Malyshev, *Phys. Lett. B* **839**, 137780 (2023).
- [52] N.A. Abdulov, A. Bacchetta, S.P. Baranov, A. Bermudez Martinez, V. Bertone, C. Bissolotti, V. Candelise, L.I. Estevez Banos, M. Bury, P.L.S. Connor, L. Favart, F. Guzman, F. Hautmann, M. Hentschinski, H. Jung, L. Keersmaekers, A.V. Kotikov, A. Kusina, K. Kutak, A. Lelek, J. Lidrych, A.V. Lipatov, G.I. Lykasov, M.A. Malyshev, M. Mendizabal, S. Prestel, S. Sadeghi Barzani, S. Sapeta, M. Schmitz, A. Signori, G. Sorrentino, S. Taheri Monfared, A. van Hameren, A.M. van Kampen, M. Vanden Bemden, A. Vladimirov, Q. Wang, H. Yang, *Eur. Phys. J. C* **81**, 752 (2021).
- [53] J. Alwall et al., *Comput. Phys. Commun.* **176**, 300 (2007).
- [54] H.Jung, S.P. Baranov, A. Bermudez Martinez, L.I. Estevez Banos, F. Guzman, F. Hautmann, A. Lelek, J. Lidrych, A.V. Lipatov, M.A. Malyshev, M. Mendizabal, S. Taheri Monfared, A.M. van Kampen, Q. Wang, H. Yang, *Eur. Phys. J. C* **81**, 425 (2021).
- [55] M. Cacciari, G.P. Salam, G. Soyez, *Eur. Phys. J. C* **72**, 1896 (2012).

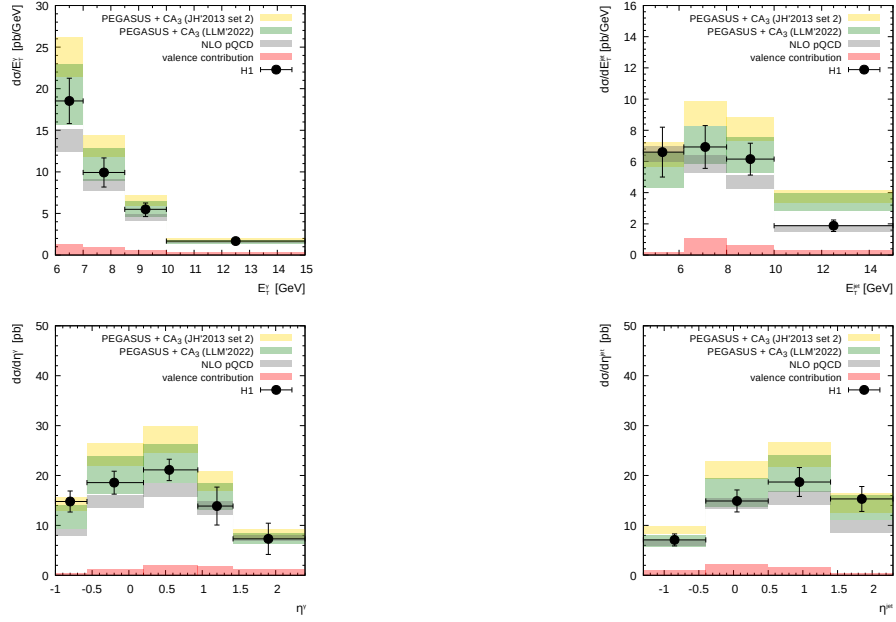


Figure 1: The associated prompt photon and jet photoproduction cross section as functions of photon and jet transverse energies and pseudorapidities. The green histograms and shaded bands correspond to the predictions obtained with LLM'2022 gluon density and estimated scale uncertainties of these calculations. The yellow histograms represent the JH'2013 set 2 predictions. Separately shown the contributions from $\gamma + q_{\text{val}} \rightarrow \gamma + q$ subprocess and conventional NLO pQCD results (taken from [1]). The experimental data are from H1 [1].

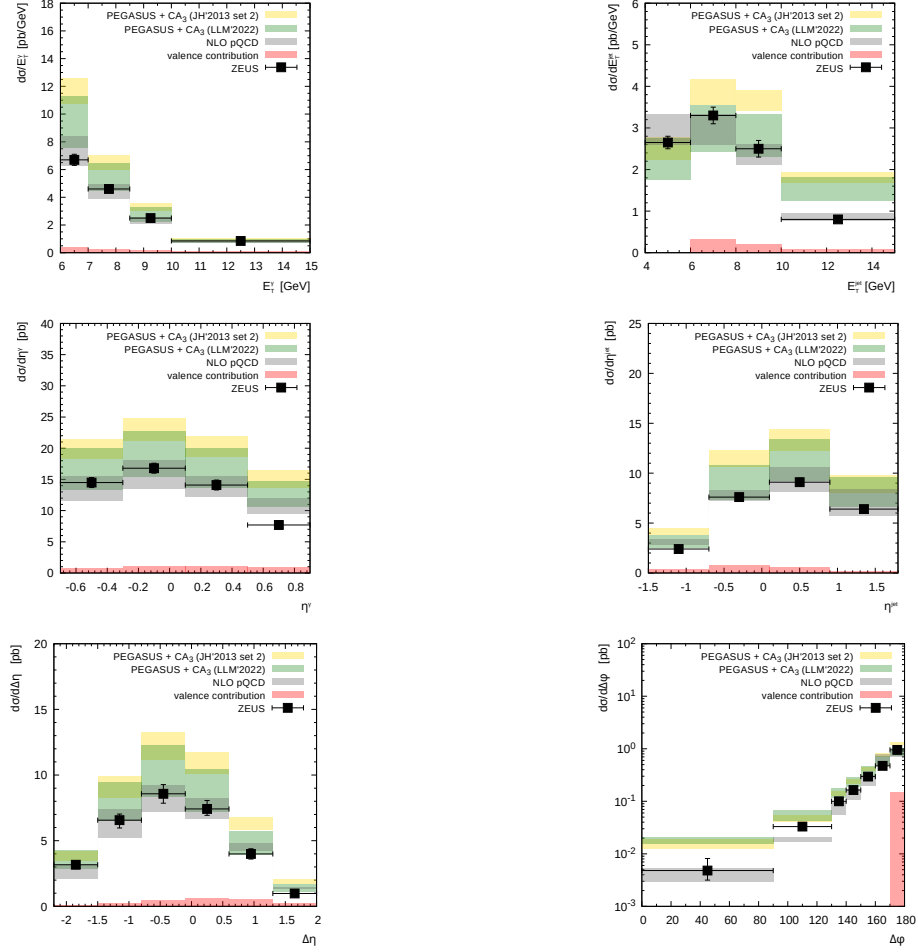


Figure 2: The associated prompt photon and jet photoproduction cross section as functions of photon and jet transverse energies, pseudorapidities, differences in their azimuthal angles and pseudorapidities. The notations are the same as in Fig. 1. The experimental data are from ZEUS [2, 3].

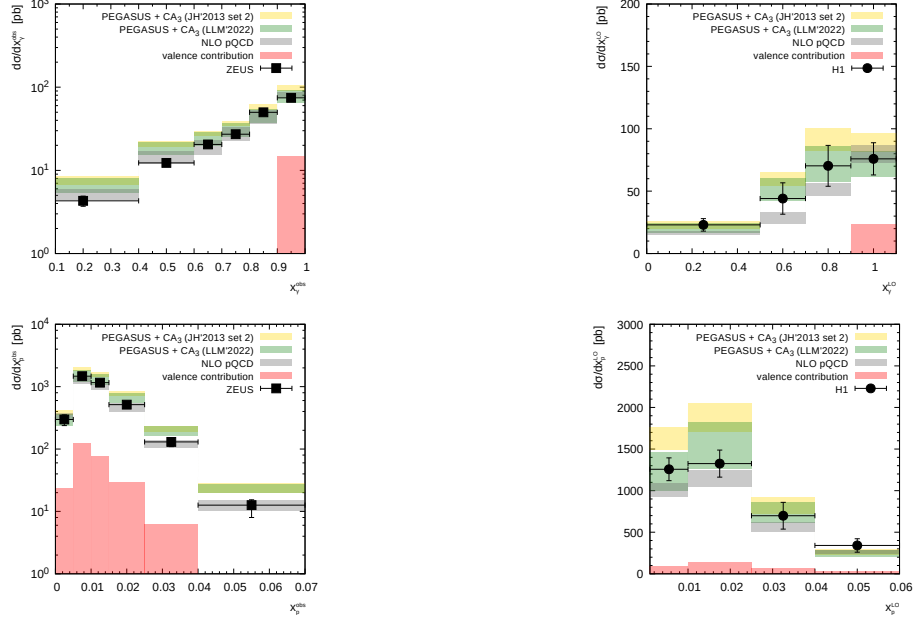


Figure 3: The associated prompt photon and jet photoproduction cross section as functions of x_γ^{LO} , x_γ^{obs} , x_p^{LO} and x_p^{obs} variables. The notations are the same as in Fig. 1. The experimental data are from H1 [1] and ZEUS [2].

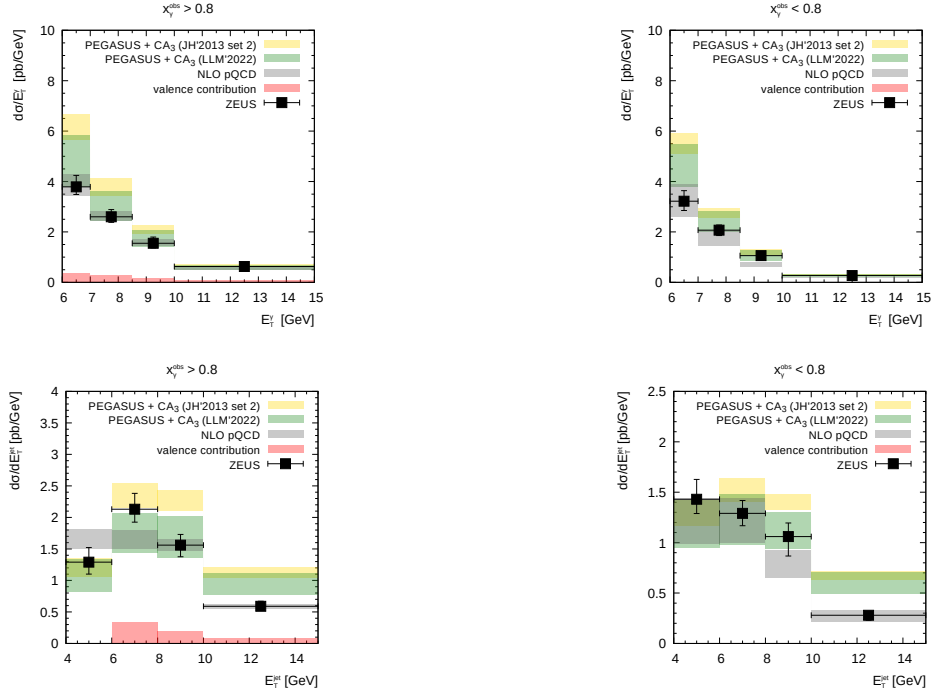


Figure 4: The associated prompt photon and jet photoproduction cross section as functions of photon and jet transverse energies E_T^γ and E_T^{jet} at $x_\gamma^{\text{obs}} > 0.8$ (left panels) and $x_\gamma^{\text{obs}} < 0.8$ (right panels). The notations are the same as in Fig. 1. The experimental data are from ZEUS [3].

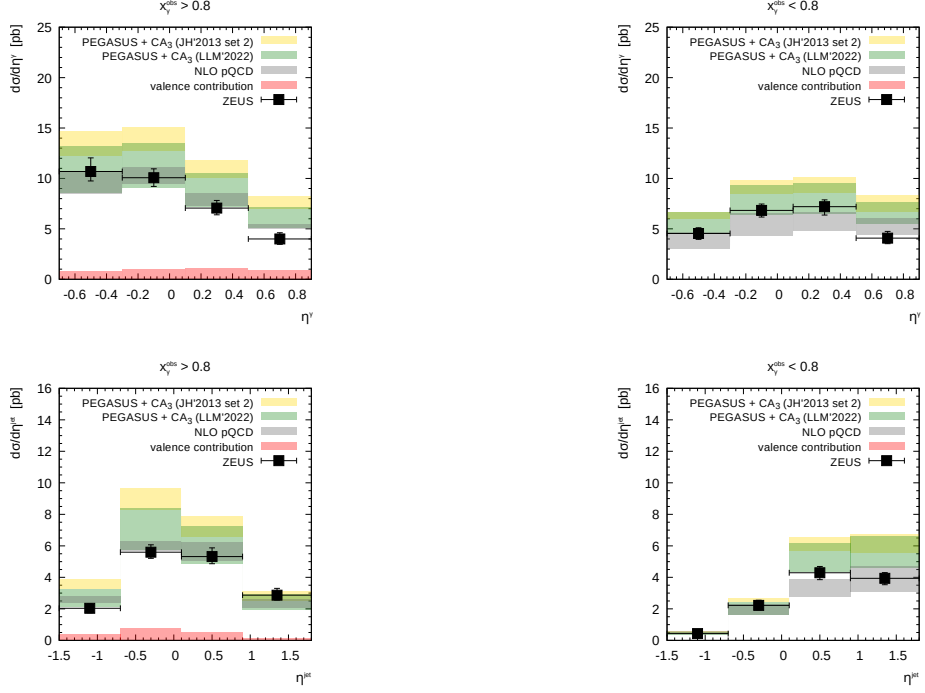


Figure 5: The associated prompt photon and jet photoproduction cross section as functions of photon and jet pseudo-rapidities η^γ and η^{jet} at $x_\gamma^{\text{obs}} > 0.8$ (left panels) and $x_\gamma^{\text{obs}} < 0.8$ (right panels). The notations are the same as in Fig. 1. The experimental data are from ZEUS [3].

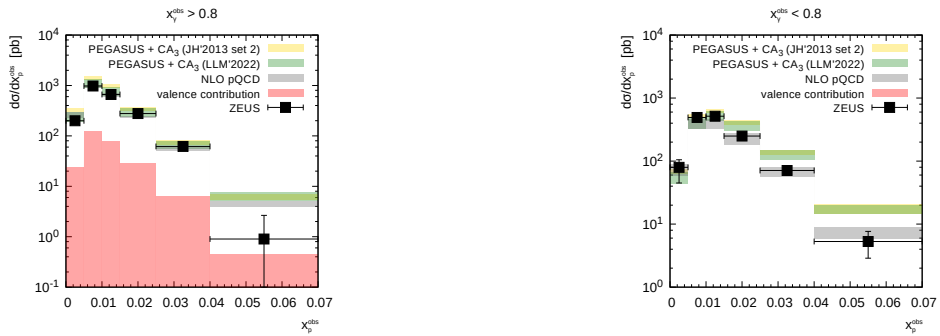


Figure 6: The associated prompt photon and jet photoproduction cross section as functions of x_p^{obs} at $x_\gamma^{\text{obs}} > 0.8$ (left panels) and $x_\gamma^{\text{obs}} < 0.8$ (right panels). The notations are the same as in Fig. 1. The experimental data are from ZEUS [3].

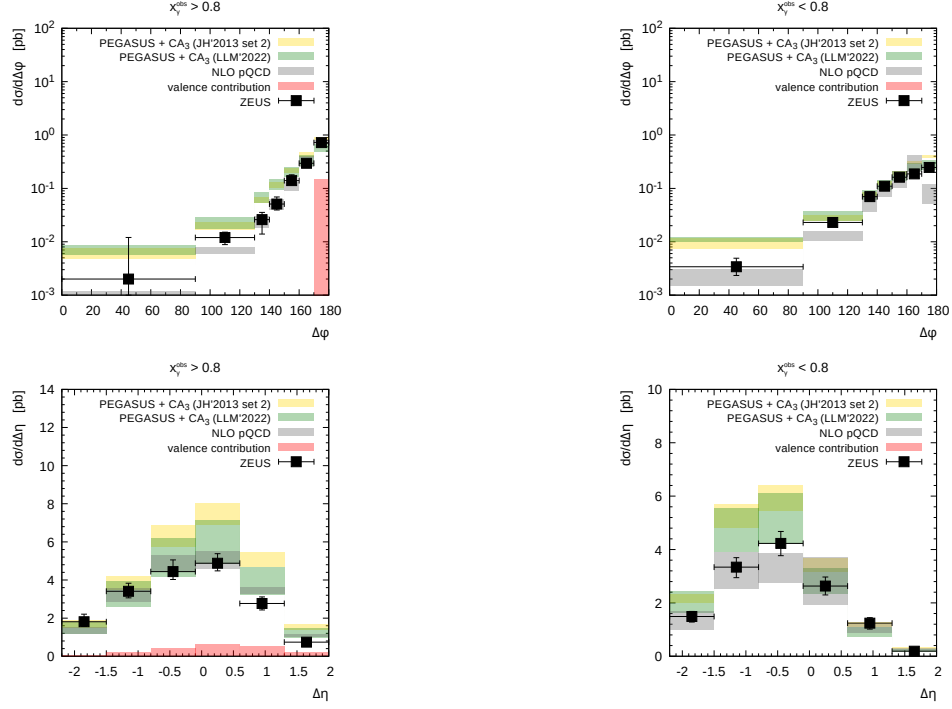


Figure 7: The associated prompt photon and jet photoproduction cross section as functions of the prompt photon and jet azimuthal angle and pseudorapidity differences $\Delta\phi$ and $\Delta\eta$ at $x_{\gamma}^{\text{obs}} > 0.8$ (left panels) and $x_{\gamma}^{\text{obs}} < 0.8$ (right panels). The notations are the same as in Fig. 1. The experimental data are from ZEUS [3].

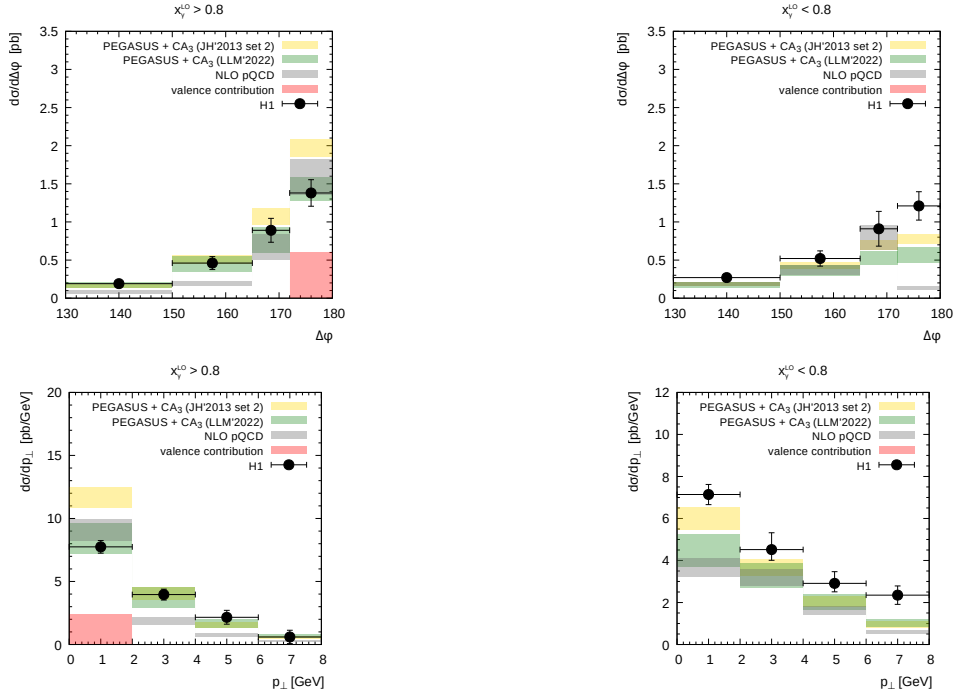


Figure 8: The associated prompt photon and jet photoproduction cross section as functions of photon and jet azimuthal angle difference $\Delta\phi$ and photon momentum perpendicular to the jet direction p_{\perp} at $x_{\gamma}^{\text{LO}} > 0.8$ (left panels) and $x_{\gamma}^{\text{LO}} < 0.8$ (right panels). The notations are the same as in Fig. 1. The experimental data are from H1 [1].